Effect of Boron on the Microstructure of Low-Carbon Steel Resistance Seam Welds

Small levels of boron in steel lead to hard weld metal microstructure and therefore must be considered in a weld specification

BY S. S. BABU, G. M. GOODWIN, R. J. ROHDE AND B. SIELEN

ABSTRACT. Small levels of boron (20–40 wt ppm) in steel were found to have a large influence on the microstructure and hardness of resistance seam welds. The decomposition kinetics of austenite to ferrite were retarded and resulted in the formation of bainitic and martensitic microstructures in the weld metal. The welds with low and high boron concentrations showed large differences in hardness. This microstructure development is in agreement with theoretical calculations of time-temperature-transformation diagrams. This work stresses the importance of considering boron levels in steels on the weld properties.

Introduction

The resistance seam welding process for steel sheets is well established. It is possible to produce high-quality welds with proper welding parameters such as electrode geometry, wheel force, weld time, welding current and contact overlap (Ref. 1). This process is being extensively used to fabricate heat exchanger panels used in electrical transformers. The welding parameters are designed to produce defect-free liquid-tight joints with the desired weld geometry. Besides the physical attributes, the strength of these welds needs to be maintained at constant level. The strength of the welds is related to the microstructural evolution during welding. In turn, the microstructural evolution in these welds depends on the steel composition and the weld thermal cycle. For example, for a given steel composition, faster weld cooling will lead to harder microstructural constituents such as bainite and martensite. In contrast, slow weld cooling will lead to soft ferritic microstructures (Ref. 2). Therefore, for a given steel composition and welding procedure specification, the microstructure and properties in weld metal and the heat-affected-zone (HAZ) are expected to be similar.

However, in routine weldability evaluations of two similar steels from different suppliers, anomalous weld microstructural evolution was observed. For similar welding conditions, one of the steels exhibited soft ferritic microstructure and the other steel exhibited hard bainitic and martensitic microstructure. This work evaluates the reasons for the above effect.

Experimental

Two hot-rolled steel sheet materials (A and B), procured to the same specification (Table 1) and used for fabrication of heat exchanger weld panels, were assessed. The actual composition of these steels is given in Table 1. The composition of the steels was measured by standard spectroscopic techniques. Boron chemical analyses were validated by comparing with NIST standards. The steel sheets were welded in a resistance seam welding machine after standard industry cleaning practice. The welding parameters were as follows: material thickness, 1.5 mm; wheel force, 6227–7562 N (1400–1700 lb); contact area of wheels, 19 x 7.62 mm (0.75 x 0.3 in.); welding current, 18,000–20,000 A; welding speed, 3.2 m/min^{-1} (126 in./min^{-1}).

Transverse sections of the welds were characterized with optical microscopy. The samples were etched with 2% Nital solution. The hardness (Vickers pyramid hardness) variations across the weld and the base metal were measured using a commercial automatic hardness tester. The hardness indents were made at equal intervals of 150 pm over an area of 6000 x 600 pm with 200-g force.

To evaluate austenite-to-ferrite decomposition in a controlled thermal cycle, Gleeble thermal simulation was performed. Small rectangular specimens were cut from the steel sheets and subjected to thermal simulation. The samples were heated to an austenitizing temperature of 1000°C and were allowed to cool at a rate of ~70°C s^{-1}. However, no artificial cooling method was used to maintain the specified cooling rate. Due to the evolution of the heat of transformation, a sudden change in the actual cooling rate of the sample was observed. To monitor such change, the actual temperature of the sample was monitored continuously during cooling. The temperature at which this change occurs is taken as the austenite-to-ferrite decomposition start temper-

KEY WORDS

Resistance Seam Welds
Low-Carbon Steel
Decomposition Kinetics
Austenite
Ferrite
Boron
Time-Temperature-Transformation Diagrams

S. S. BABU and G. M. GOODWIN are with Metals and Ceramics Division, Oak Ridge National Laboratory, Oak Ridge, Tenn. R. J. ROHDE and B. SIELEN are with Waukesha Electric Systems, Waukesha, Wis.

Table 1—Steel Compositions (wt-%)

Element	Specification	Steel A	Steel B
C	0.01–0.10	0.031	0.059
Mn	0.15–0.40	0.20	0.22
P	0.035 maximum	0.007	0.008
S	0.020 maximum	0.011	0.004
Si	Not specified	0.01	0.01
Ni	Not specified	0.01	0.03
Cr	Not specified	0.02	0.02
Al	Not specified	0.031	0.036
V	Not specified	0.001	0.001
Ti	Not specified	0.001	0.001
B	Not specified	<0.0005[a] (5 wt. ppm)	0.002–0.004[b] (20–40 wt.% ppm)
N	Not specified	0.004	0.004
Fe	Balance	Balance	Balance

(a) Below detectable level, that is 5 wt. ppm.
(b) Boron levels are validated by comparing with NIST standards. The range was encountered in different locations in Steel B.

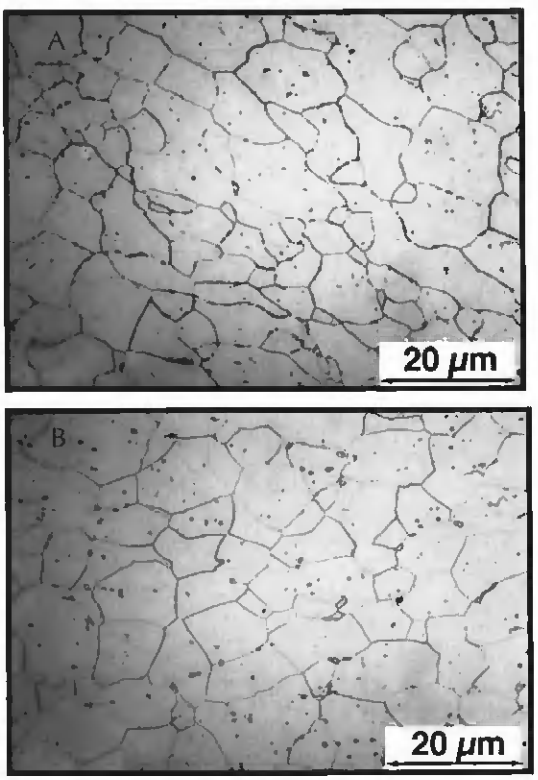

Fig. 1 — Comparison of base metal microstructure. A — Steel A; B — Steel B.

ature; the lower the transformation start temperature, the higher the possibility for the formation of hard bainitic and martensitic microstructures.

To understand and delineate the effect of steel composition on austenite-to-ferrite decomposition kinetics, the time-temperature-transformation (TTT) diagrams were calculated using a published model (Ref. 3). It is important to note that the diagrams are not specific to heat-affected zone or fusion zone. These diagrams give an overview of austenite-to-ferrite decomposition behavior. The model allows one to calculate the time (t) for the initiation of ferrite transformation from austenite. This time is related to the chemical driving force for nucleation of ferrite, which is a function of weld metal composition (C, Si, Mn, Ni, Cr and Mo) and temperature. The reader is directed to Ref. 3 for more details[1]. Thermodynamic calculations with ThermoCalc software (Ref. 4) were performed to estimate the solid soluble concentration of boron. The TTT diagrams are then used to calculate the continuous cooling transformation (CCT) diagrams using the additivity rule (Ref. 5).

Results and Discussion

Microstructural Characterization

The base metal microstructures of Steels A and B are compared in Fig. 1. There is no distinct difference either in ferrite grain size or ferrite morphology. This is expected because both steels were manufactured by a standard hot rolling operation. The hardness of Steel A was found to be 113±7 VPH and that of Steel B was found to be 119±11 VPH. This shows that both the steels have essentially identical strength levels. Since the compositions of Steels A and B (Table 1) are similar, the microstructure and properties of the welds might be expected to be the same.

However, the macro- and microstructure of seam welds in Steels A and B showed major differences — Fig. 2. The weld nugget size of Weld B was found (based on many transverse sections) to be larger than Weld A. The reason for the large weld zone is not clear. It is speculated that the contact resistance of Steel B may be higher than Steel A and might have resulted in larger nuggets. Further work is necessary to understand the nugget formation in these two steels. This difference in nugget size is expected to change the microstructural evolution by altering the thermal cycle.

Since the weld nugget size of Weld B is larger than Weld A, the cooling rate in Weld B is expected to be lower than in Weld A. This difference in cooling rate is expected to produce softer ferritic microstructure in Weld B. However, contradictory microstructural results were observed. Careful observation of Weld B at high magnification (Fig. 2D) revealed predominantly bainitic and martensitic microstructure in the weld metal region. In contrast, the microstructure of Weld A (Fig. 2C) contained predominantly allotriomorphic ferrite and small amounts of bainite and martensite in the weld metal region. Optical microscopy revealed no significant difference in prior austenite grain size between the welds. In the fusion zone region, in all the locations, there was a negligible amount of allotriomorphic ferrite along the austenite grain boundary. Besides the microstructural differences, the hardness measurements also showed differences between Welds A and B. The hardness values across the weld region are compared in Fig. 3. The measured area extended over the base metal, the heat-affected zone and the weld zone. The plot shows that the weld metal region in Weld B is harder than in Weld A. The above microstructural and hardness variations indicate that, even with slow cooling rates and similar steel compositions, Weld B consists of harder bainitic and martensitic microconstituents.

The above result apparently contradicts the well-established fact that a slower weld cooling rate will lead to a softer ferritic microstructure for a given steel composition. Since there was uncertainty in the weld thermal cycle experienced by Welds A and B during resistance seam welding, the austenite-to-ferrite transformation temperature was studied during simulated cooling conditions. Moreover, predictive models were used to estimate the austenite-to-ferrite decomposition behavior as a function of steel composition.

Gleeble Thermal Simulation

Both Steels A and B were programmed to identical thermal cycling. The actual on-cooling temperatures of

1. The calculations can be accessed via the World Wide Web at http://engm01.ms.ornl.gov.

the samples were measured during the cooling cycle — Fig. 4. With the initiation of transformation, the heat of transformation is released. This heat reduces the cooling rate of the sample because there are no artificial cooling methods in the present experiment. The transformation start temperatures (at which the change in cooling rate occurs) were derived from these measurements. The transformation start temperature of Steel A is found to be ~820°C and that of Steel B ~700°C. The results demonstrate that the hardenability of Steel B is higher than that of Steel A. Therefore, it is necessary to delineate the possible cause for this difference.

Calculation of Austenite-to-Ferrite Decomposition

The austenite decomposition kinetics are influenced by the concentration of various elements including C, Mn, Ni, Si, Cr, Mo and B. Careful examination of the composition of Steels A and B showed differences in concentrations of C, Mn, P, S, Ni and B. The small differences in concentrations of Mn, P, S and Ni are not expected to change the decomposition kinetics to a great extent (Ref. 3); however, it is well known that small changes in C and B may have a large influence on the austenite-to-ferrite decomposition kinetics (Ref. 6). The effect of various elements on the austenite-to-ferrite decomposition can also be inferred from carbon equivalent formulas (Ref. 7). The original model developed by Bhadeshia (Ref. 3) allows one to estimate the TTT diagrams for a steel composition as a function of C, Si, Mn, Ni, Cr and Mo concentration. In this model, the effect of boron was not considered. Therefore, the calculations for Steels A and B (Fig. 5) will reflect only the effect of small differences in carbon concentration. The plot shows that the difference in carbon concentration does not change the TTT behavior significantly. Previous work by Bhadeshia, *et al.* (Ref. 8), has shown that the growth rate of ferrite can be suppressed a to large extent by increasing carbon concentration, thereby reducing allotriomorphic ferrite fractions. Allotriomorphic ferrite thickness was estimated for both Steels A and B, for a dwell time of 1 s at 700°C, with the method given in Ref. 8. As expected, the calculated ferrite thickness for Steel A was 6.2 μm and that of Steel B was 3.6 μm. However, in the present work, the Steel B welds showed a negligible amount of allotriomorphic ferrite. Therefore, the change in carbon may not be sufficient enough to induce the observed difference in weld microstructure.

Recently, the original TTT model has been modified by Bhadeshia and Svensson (Ref. 9) to consider the boron effect. In this model, the initiation of transformation to allotriomorphic ferrite from austenite is retarded as a function of boron concentration in solid solution in the austenite. In their work, the boron in solid solution was estimated by considering thermodynamic equilibrium between austenite, TiN and BN at 900°C. Moreover, above 10 wt ppm boron in solution, the boron effect was found to be constant. In the present experiment, the amount of boron in solution will depend on the austenitization temperature. To estimate the boron in solution within the austenite, equilibrium calculations were performed with ThermoCalc. Recently, Bang and Ahn (Ref. 10) also estimated the soluble boron by solving the solubility equations of TiN, AlN and BN. However, in this work, the phase equilibria between austenite, carbonitrides (Ti,V|C,N|), AlN and BN were considered and it allowed for estimation of the volume fractions of these phases. The calculated boron concentrations in solution as a function of temperature for Steels A and B, with different nominal boron levels, are shown in Fig. 6. The boron in solution for the austenitizing temperature of 1000°C for Steel B (with 20 wt ppm B) was found to be 0.34 wt ppm. In contrast, if the nominal concentration of boron is 40 wt ppm B, the boron in solution increases to 10 wt ppm. Both 20 and 40 wt ppm boron were measured in different locations in Steel B. The nominal concentration of boron in Steel A was assumed to be S wt ppm because the concentration below S wt ppm of boron could not be detected experimentally. With this assumption, the boron

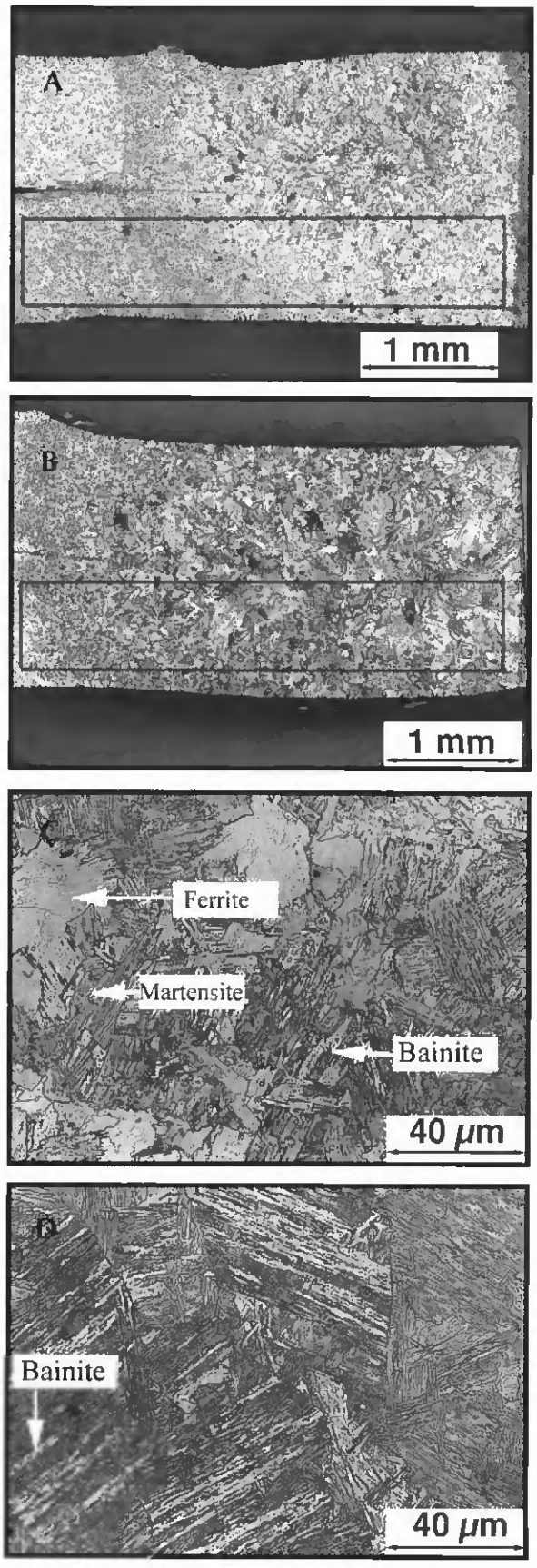

Fig. 2 — Comparison of weld microstructure of Welds A and B. A and B — Macrostructure; C and D — microstructure. (The white rectangular boundary shows the region of hardness measurements.)

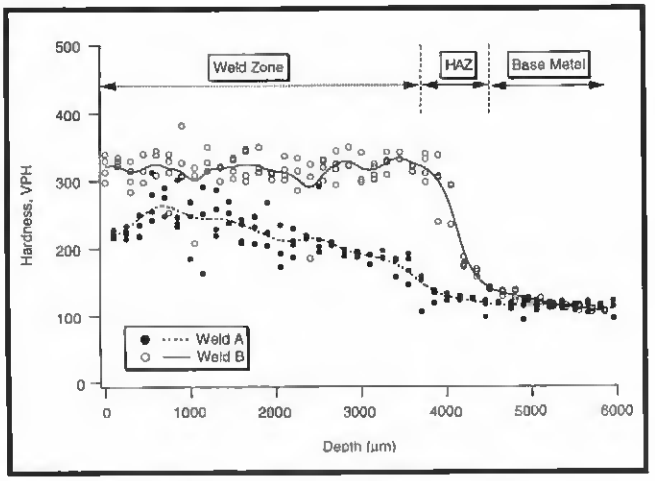

Fig. 3 — Comparison of Vickers pyramid hardness variations in Welds A and B. The plots indicate a harder weld zone in Weld B than in Weld A.

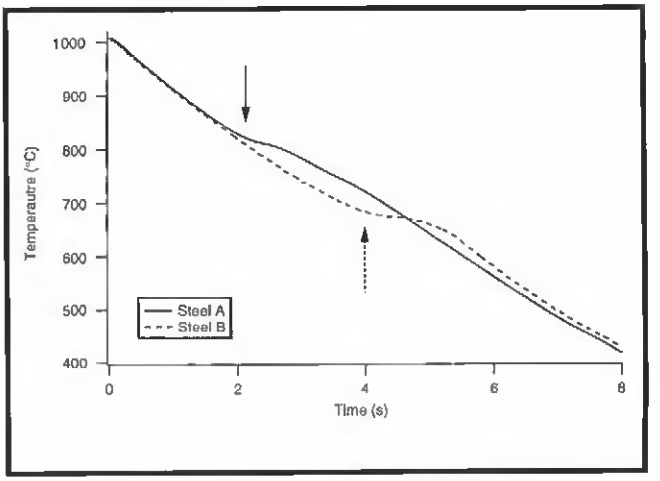

Fig. 4 — The variation of actual temperature with time for Steels A and B during cooling from 1000°C. The change of slope (marked by arrows) indicates the transformation start temperature.

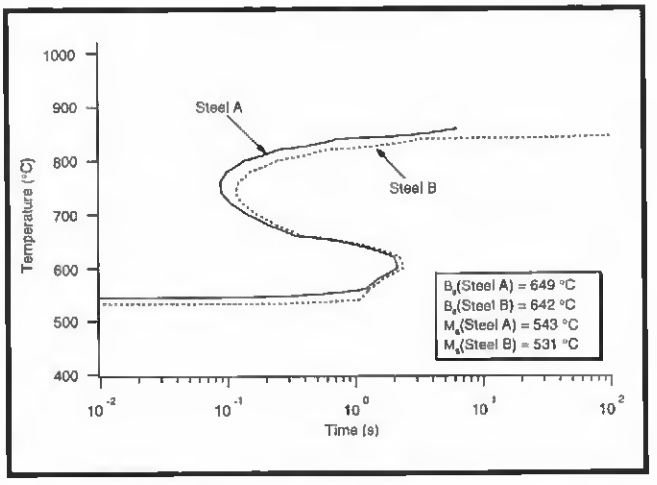

Fig. 5 — Calculated diagram for initiation of transformation for Steels A and B, without considering the boron effect. The bainite start (B_s) and martensite start (M_s) were obtained from the TTT model (Ref. 3). The calculations consider the effect of C, Si, Mn, Ni, Mo and Cr concentrations.

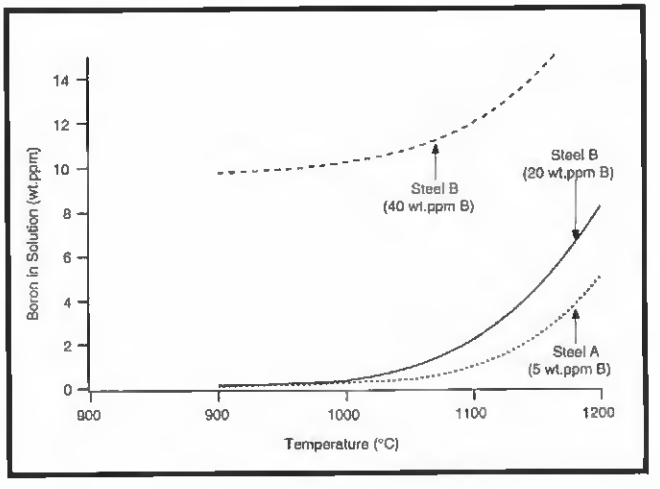

Fig. 6 — Calculated boron concentration (wt ppm) in solid solution within austenite for Steel A (with 5 wt ppm boron) and B (with 20 and 40 wt ppm boron) as a function of temperature.

in solution in Steel A for the austenitizing temperature of 1000°C was found to be 0.24 wt ppm. The above estimates were used to calculate the modified TTT diagrams — Fig. 7.

The calculations demonstrate that the small boron level in Steel B retards the austenite-to-ferrite decomposition kinetics. The initiation time for ferrite formation is retarded to such an extent that austenite decomposition will occur at significantly lower temperatures. This will lead to large fractions of bainite and martensite in Steel B for similar thermal cycles. The diagrams for Steels A and B were converted into CCT diagrams (Fig. 8) assuming linear cooling rates from 0.1 to 10,000 Cs^{-1}. The CCT calculations compare very well with the experimentally measured transformation start temperatures. The experimental transformation start for Steel A was found to be in between the one calculated for 0 and 5 wt ppm of boron. The experimental transformation start for Steel B was found to be in between the one calculated for 20 and 40 wt ppm of boron.

In the above calculations, the boron in solution was calculated for the austenitizing conditions. In the case of continuously cooled weld metal, the boron in solution would vary as the weld cools. The precipitation of AlN, BN and Ti,V(C,N) may occur at higher temperature. Therefore, the amount of boron in solution will depend on the thermodynamic equilibrium at or near the transformation start temperatures. Bhadeshia, *et al.* (Ref. 9), assumed this temperature to be 900°C irrespective of the steel composition.

Significance of the Results

The above results demonstrate the importance of boron on microstructural evolution. Small amounts of boron coupled with rapid cooling conditions can induce hard bainitic and martensitic microstructure even in very low-carbon steel welds. These microstructural changes will result in large differences in properties. It is important to note that the specifications for typical steels used for resistance welds do not specify the boron levels. Therefore, for consistent weld quality considerations, it is recom-

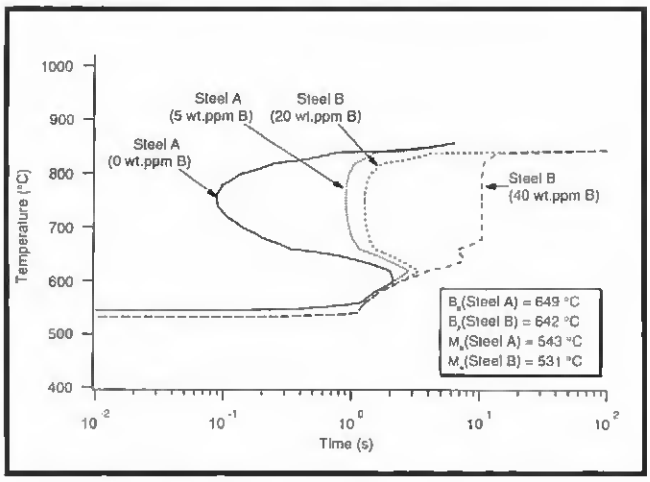

Fig. 7 — Calculated diagram for initiation of transformation of Steels A (with no boron and assumed 5 wt ppm boron) and B, with 20 and 40 wt ppm boron. It is important to note that the change in TTT diagrams are based on soluble boron in the austenite calculated by ThermoCalc.

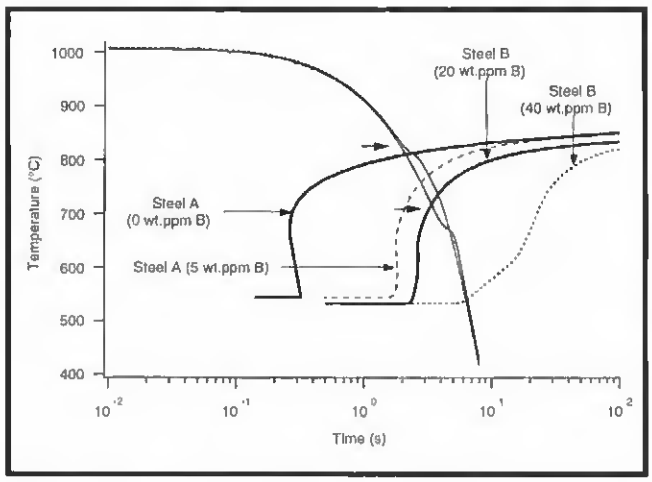

Fig. 8 — Calculated CCT diagram for initiation of transformations in Steels A and B. The CCT lines for steel A with 0 and 5 wt ppm B and Steel B with two boron levels are shown. The temperature-time data measured for Steels A and B in Gleeble simulation are also shown. The arrows indicate the approximate transformation temperatures.

mended that boron levels in steels be considered. Moreover, with increased use of recycled steels, it is important to quantify and evaluate the effects of other elements in steels. In this context, one needs to consider austenite grain size variations on the microstructure development.

Additionally, to avoid the formation of hard bainitic and martensitic microstructures in welds, the welding parameters can be modified. The modifications can induce a slow cooling in the temperature range of allotriomorphic ferrite formation. This will reduce the bainite and martensite fraction in the microstructure. Currently, at Oak Ridge National Laboratory (ORNL), a comprehensive thermal-microstructure-property model is being developed to optimize the welding parameters for the required weld properties.

Conclusions

Two steels with similar strength levels welded by the resistance seam welding process exhibited large differences in microstructure and hardness. These differences were attributed to the sluggish austenite decomposition kinetics in the steel with higher boron. This resulted in the formation of bainitic and martensitic constituents and a hard weld zone. In contrast, the steel with low boron level transformed predominantly to allotriomorphic ferrite and resulted in a comparatively softer weld zone. The results are supported by Gleeble thermal simulation results. Theoretical continuous cooling transformation predictions, considering the effect of soluble boron, compare very well with the experimentally measured transformation behavior.

Acknowledgments

Research sponsored by the U.S. Department of Energy, Division of Materials Sciences, and Assistant Secretary for Energy Efficiency and Renewable Energy, Office of Industrial Technologies, Metals Processing Laboratory User Center (MPLUS), Advanced Industrial Materials Program, under contract DE-AC05-96OR22464 with Lockheed Martin Energy Research Corp. The authors thank M. W. Richey of LMES, Oak Ridge, and J. F. King of ORNL for helpful discussions. The authors also thank D. A. Frederick for help with Gleeble thermal simulations and A. Nation of ABB Combustion Inc., Chattanooga, Tenn., for performing residual boron analyses.

References

1. Welding Processes. *Welding Handbook*, Vol. 2, 8th ed 1991. Ed. R. L. O'Brien. American Welding Society, Miami, Fla. p. 552.

2. Ion, J. C., Easterling, K. E., and Ashby, M. F. 1984. A second report on diagrams of microstructure and hardness for heat-affected zones in welds. *Acta. Metall.*, 32: 1949–1962.

3. Bhadeshia, H. K. D. H. 1982. A thermodynamic analysis of isothermal transformation diagrams, *Metal Science*, 16: 159–165.

4. Sundman, B., Jansson, B., and Andersson, J.-O. 1985. The ThermoCalc databank system. *Calphad*, 9: 153–190.

5. Babu, S. S. 1991. Acicular ferrite and bainite in Fe-Cr-C weld deposits. Ph.D. dissertation. Cambridge, U.K. University of Cambridge.

6. Pickering, F. B. 1978. Physical metallurgy and the design of steels. *Applied Science*, U.K.

7. Yurioka, N. 1995. TMCP steels and their welding. *Welding in the World*, 35: 2–17

8. Bhadeshia, H. K. D. H., Svensson, L.-E. 1985. A model for development of microstructure in low-alloy steel (Fe-Si-Mn-C) weld deposits. *Acta Metall.*, 33: 1271–1283.

9. Bhadeshia, H. K. D. H., and Svensson, L.-E. 1993. Model for boron effects in steel welds. *Proc. International Conference on Modeling and Control of Joining Processes*, ed. T. Zacharia, pp. 153–160. American Welding Society, Miami, Fla.

10. Bang, K-s., and Ahn, Y-h. 1997. Weldability of direct-quenched, low-carbon T-B-containing steels. *Welding Journal*, 76(4): 151-s to 157-s.